Microbial life and biogeochemical cycling on land 3,220 million years ago

Martin Homann, Pierre P Sansjofre, Mark van Zuilen, Christoph Heubeck,
Jian Gong, Bryan Killingsworth, Ian Foster, Alessandro Airo, Martin van
Kranendonk, Magali P Ader, et al.

1 # Microbial life and biogeochemical cycling on land 3,220 million years ago

2 Martin Homann[1*], Pierre Sansjofre[1], Mark Van Zuilen[2], Christoph Heubeck[3], Jian Gong[2],

3 Bryan Killingsworth[1], Ian S. Foster[1], Alessandro Airo[4], Martin J. Van Kranendonk[5], Magali

4 Ader[3], and Stefan V. Lalonde[1]

5

6 [1]European Institute for Marine Studies, CNRS-UMR6538 Laboratoire Géosciences Océan,

7 Technopôle Brest-Iroise, Place Nicolas Copernic, 29280 Plouzané, France. *corresponding author:

8 martin.homann@univ-brest.fr

9 [2] Institut de Physique du Globe de Paris, CNRS-UMR7154, 4 place Jussieu, 75005 Paris, France

10 [3] Department of Geosciences, Friedrich-Schiller-Universität, Burgweg 11, 07749 Jena, Germany

11 [4]Center of Astronomy and Astrophysics, Technische Universität Berlin, Straße des 17. Juni 136,

12 10623 Berlin, Germany

13 [5]Australian Centre for Astrobiology, and School of Biological, Earth and Environmental Sciences,

14 University of New South Wales, Sydney, NSW, 2052, Australia.

15
16

17 **The colonization of emergent continental landmass by microbial life was an evolutionary**

18 **step of paramount importance in Earth history. Here we report direct fossil evidence for**

19 **life on land 3,220 Myr ago in the form of terrestrial microbial mats draping fluvial**

20 **conglomerates and gravelly sandstones of the Moodies Group, South Africa. Combined**

21 **field, petrographic, carbon isotope, and Raman spectroscopic analyses confirm the**

22 **synsedimentary origin and biogenicity of these unique fossil mats as well as their fluvial**

23 **habitat. The carbon isotope composition of organic matter ($\delta^{13}C_{org}$) from these mats**

24 **define a narrow range centered on -21‰, in contrast to fossil mats of marine origin from**

25 **nearby tidal deposits that show $\delta^{13}C_{org}$ values as low as -34‰. Bulk nitrogen isotope**

26 **compositions ($2<\delta^{15}N<5‰$) are also significantly different from their marine counterparts**

27 **($0<\delta^{15}N<3‰$), which we interpret to reflect denitrification in the terrestrial habitat,**

28 **possibly of an atmospheric source of nitrate. Our results support the antiquity of a**

29 **thriving terrestrial biosphere during the Paleoarchean and suggest that a complex and**

30 **microbially-driven redox landscape existed during the deposition of the Moodies Group,**

31 **with distinct biogeochemical cycling occurring on land by 3,220 Myr ago.**

32
33

34 While there is abundant evidence that microbial life thrived in the oceans as far back as there

35 is a sedimentary record[1–5], significantly less is known about microbial colonization of the land

36 surface. Before 3,000 Myr ago, much of the Earth may have been submerged[6], and accordingly,

37 direct fossil evidence for terrestrial[7] life prior to the Mesoarchean is extremely rare[8,9]. It is also

inferential, largely derived from the study of paleosols as old as 3,200 Myr[10–14]. A suite of suggestive biosignatures in hot spring deposits indicate that life may have already been occupying terrestrial niches by 3,480 Myr[15]. Here we present the discovery of a new locality in the Paleoarchean Moodies Group, Barberton Greenstone Belt (BGB), South Africa, where exceptionally-preserved microbial mats are exposed in sediments of an ancient fluvial system. These terrestrial fossils represent a significant expansion of the known diversity of microbial life in the Moodies Group, which until now has been restricted solely to marine settings[16–20].

The Moodies Group is the uppermost of the three stratigraphic units constituting the Barberton Greenstone Belt (Supplementary Fig. 1) and represents the world's oldest well-preserved alluvial to shallow marine deposit[21,22]. It consists of a thick (up to 3.5 km) succession of alluvial to shallow-marine quartz-rich sandstones with subordinate conglomerates, mudstones, thin tuffs, banded iron formations, and a single basaltic lava[22]. The age of the Moodies Group is tightly constrained by several dacitic tuffs and rare felsic dikes radiating from the Kaap Valley tonalite that crosscut the Moodies Group along the northern margin of the BGB. U-Pb dating of single-zircons from these units indicate that deposition began about 3,223 ± 1 Myr and had ended by about 3,219 ± 9 Myr[23,24]. The southwestward-plunging Dycedale Syncline, approx. 2 km east of Barberton, hosts a steeply dipping >350 m thick succession of Moodies Group conglomerates and cross-bedded sandstones. A large variety of sedimentary structures indicates that this succession records a transition from alluvial-fluvial (terrestrial) to tide-influenced marine sedimentation[21,22] (Supplementary Fig. 2).

Terrestrial microbial mats in fluvial sandstones

Our study is focused on fossilized microbial mats discovered in this unique terrestrial-to-marine transition in the Dycedale Syncline. The base of the section begins with a ~75-m-thick sedimentary unit including a ~40 m thick, polymict, mostly clast-supported conglomerate in

64   the central part (unit B of ref. 22; Supplementary Fig. 2). The poor sorting and angularity of

65   clasts, poorly developed internal fabrics, clast imbrication, thin intercalated sandstone beds with

66   upper-plane bed horizontal lamination, and the immature composition of this conglomerate

67   indicate a proximal sediment source associated with episodic, short-lived, high-energy

68   unidirectional transport. These fabrics and associations are typical for sheet flow-dominated

69   alluvial fans and/or proximal braided streams with highly variable discharge. The conglomerate

70   is under- and overlain by 10- and 25-m-thick (respectively) gravelly sandstones with

71   carbonaceous laminations and minor interbedded conglomerate beds. These lens- or wedge-

72   shaped beds are 0.2 to 2 m thick, commonly vertically stacked, and show minor channel incision

73   from erosional downcutting, characteristic of fluvial deposition and transport (Fig. 1a). Pebble-

74   to boulder-sized clasts (up to ~40 x 40 cm) are subrounded, poorly-sorted, and embedded in a

75   quartz-rich coarse-sandy matrix (Fig. 1b). The transition to overlying gravelly, medium- to

76   coarse-grained quartzofeldspathic sandstones is gradational. These horizontal to low-angle

77   planar cross-bedded sandstones are locally interbedded with discontinuous mudstones with

78   desiccation cracks, indicating periods of subaerial exposure (Supplementary Fig. 3). Overlying

79   strata gradually deepen upward through deltaic, and medium-energy tidal, into subtidal

80   siliciclastic deposits. The position of the conglomerate-bearing deposits at the base of this

81   transgressive, fining- and deepening-upward sequence, and the absence of any sedimentary

82   structure indicative of tidal or marine conditions, further suggests that the gravelly sandstones

83   and conglomerates represent a terrestrial depositional environment, likely a fluvial coastal

84   braidplain that was updip of an estuary[22].

85

86   The wavy and crinkly carbonaceous laminations within these gravely sandstones and on top of

87   the conglomerate beds show a variety of features consistent with a biogenic origin. They are

88   densely spaced at the mm-scale, and both onlap and drape protruding clasts (Fig.1c-d). Laminae

89   are bent upwards and plastically deformed by 10- to 50-cm-high subvertical fluid-escape

3

structures, indicating their cohesive water-impermeable nature and synsedimentary origin (Fig. 1e, Supplementary Fig. 4). A high strength and cohesiveness of the laminae is further supported by their association with coarse-grained sandstone and conglomerate beds that were repeatedly emplaced on top of the laminae without severely damaging or eroding them (Fig. 2a). However, petrographic analysis also reveals that during periods of increased current velocity, and therefore higher shear stress, laminae were partially eroded, ripped up and reworked as fragments of up to several cm in length (Fig. 2a and 2c-f). In thin section, the 0.5 - 4 mm thick laminae are composed of a dense meshwork of interwoven filament-like microstructures that drape horizontally laminated and rippled sandstones, onlap individual clasts, and envelop "floating" detrital grains of fine-grained sand whose long axes are preferentially aligned parallel to bedding (Fig. 2a-b). Individual carbonaceous filamentous structures are 1 - 3 μm in diameter and may exceed 100 μm in length, commonly bundled and twisted around each other (Fig. 2c; Supplementary Fig. 5), consistent with, but not exclusive to, modern filamentous microorganisms forming biofilms. The excellent preservation of these features is thought to be due to a combination of very early silicification, low tectonic strain, and the low temperature of post-depositional hydrothermal overprinting (<150°C) in the interior part of the Barberton Greenstone Belt[19,25]. Raman microspectroscopy demonstrates that the carbonaceous laminae of both the terrestrial and marine mats[19] are composed of organic carbon that has experienced similar peak temperatures of ~365°C (see Methods), consistent with the metamorphic grade of lower greenschist facies established by mineralogical indicators[26] and previous Raman-based estimates of regional peak metamorphic temperatures for the central part of the BGB[27] (Fig. 3, Supplementary Fig. 6, Supplementary Table 1). This confirms that the laminae are of syngenetic origin with the sandstone. Based on the combined evidence of carbonaceous composition, syngenicity, cohesiveness, sediment trapping behavior, and the presence of filamentous microstructures, the laminae are confidently identified as the fossilized remnants of microbial mats.

4

116   The presence of microbial mats on land during the Paleoarchean provides important insights

117   into the timing of certain evolutionary innovations required for terrestrialization. The Archean

118   land surface was likely a harsh environment subject to repeated desiccation, fluvial and/or

119   aeolian abrasion, and presumably, intense UV radiation. Its colonization suggests that the

120   terrestrial mats possessed a variety of adaptations, including tolerance to high shear stresses via

121   formation of cohesive and resistive mats, production of hygroscopic EPS (extracellular

122   polymeric substance) to maintain wetting during subaerial exposure, synthesis of UV-screening

123   pigments and an enhanced capacity for DNA-repair to cope with cellular damage induced by

124   desiccation and/or exposure to high-incidence UV radiation. It appears that terrestrial mats of

125   the Moodies Group already possessed such coping mechanisms at 3,220 Myr.

126

127   Our new report of terrestrial mat fossils adds to the known diversity of the Moodies ecosystem,

128   which includes large spheroidal microfossils[16], widespread shallow marine tufted microbial

129   mats with trapped gas bubbles[17–19], and remnants of cavity-dwelling microbes thriving beneath

130   the mats[20]. These coeval marine microbial communities are preserved in sandstones in the

131   nearby Saddleback Syncline that show clear bidirectional paleocurrent patterns characteristic

132   of deposition under tidal influence[19].

133

134   To better characterize and distinguish the paleobiological context of these unique terrestrial

135   mats from their marine counterparts, we subsampled mat-rich horizons from both and analyzed

136   them for the carbon isotope composition of organic matter and for bulk nitrogen isotope

137   composition. We also examined dolomite remnants that occur as bladed to blocky cement in

138   mm- to cm-sized bedding-parallel cavities beneath the mats[19,20] in both environments. In places

139   these carbonates are plastically deforming and rupture the mats, which further indicates their

140   early diagenetic formation, prior to sandstone lithification (Supplementary Fig. 7). All

141   carbonates yielded homogeneous mean $\delta^{13}C_{carb}$ values of +0.2 ±0.2‰ and $\delta^{18}O_{carb}$ values of -

142   15.4‰ ±0.2‰ (n=16, Supplementary Table 2), common values for dolomitic carbonates of

143   Archean age that rule out significant secondary exchange between carbon pools after burial.

144

145   **Carbon fixation in Moodies Group microbial mats**

146   The carbon isotope composition of preserved organic matter provides a more direct link to

147   metabolic activity during mat growth. In the terrestrial mats, $\delta^{13}C_{org}$ values range between -

148   23.6‰ and -17.9‰, with a mean of -21.2‰ (n=36; Supplementary Table 3). These values

149   contrast with isotopically lighter $\delta^{13}C_{org}$ values of microbial communities from the coeval

150   marine deposits, ranging between -33.9‰ and -21.3‰, with a mean of -27.4 (n=30; Fig. 4).

151   The observed difference between the two data sets is statistically significant (two-tailed

152   Welsh's t-test, p<0.0001). The ~6‰ shift to heavier $\delta^{13}C_{org}$ values in the terrestrial realm thus

153   suggests significant environmental and metabolic diversity across this Paleoarchean ecosystem

154   landscape.

155

156   There are several non-mutually exclusive explanations for this shift. Firstly, cell size, growth

157   rate, and species-specific differences in CO_2 diffusion rates all influence ε_p, the carbon isotopic

158   fractionation factor associated with phototrophic carbon fixation[28,29]. However, the influence

159   of these factors on ε_p tends toward zero[29] as pCO2 approaches the elevated values inferred for

160   the Archean[30], and some bacterial species exhibit little variation even at low CO_2

161   concentrations[31]. A more likely explanation for this shift is a mixing of carbon sources with

162   different isotopic compositions. The terrestrial samples exhibit a narrow distribution in $\delta^{13}C_{org}$

163   values, suggesting a relatively homogenous source centered around -21‰. This $\delta^{13}C_{org}$

164   composition is consistent with autotrophic carbon fixation via the Calvin-Benson cycle[32,33],

165   whether by oxygenic or anoxygenic phototrophs. Marine samples reach values that are

166   isotopically as heavy, yet cover a larger spread extending to lighter $\delta^{13}C_{org}$ values, some as low

167   as -34‰. These features suggest that in the marine realm, mixing occurred between material

168   with the same isotopic composition (-21‰) as terrestrial samples and material with carbon that

169   was isotopically lighter than -34‰. Under high pCO_2, carbon fixed by the Calvin-Benson cycle

170   is unlikely to reach such low values[34], which are best explained instead by biomass derived

171   from other carbon fixation pathways, notably the reductive Acetyl Co-A (Wood–Ljungdahl)

172   pathway[34–36]. This includes acetogenic bacteria, methanogens, and sulfate reducers that, with

173   the exception of some examples of the latter[37], are obligate anaerobes. The terrestrial mat

174   samples are rather remarkable in that the light carbon isotope signature that should be associated

175   with alternative fixation pathways such as the reductive Acetyl Co-A pathway is not observed.

176

177   We suggest that this disparity reflects differences in fermentative or respiratory processes

178   occurring in the mats along a paleoenvironmental transect. One possibility is that higher

179   sedimentation rates in the terrestrial realm promoted rapid burial of carbon formed at the mat

180   surface via the Calvin-Benson pathway, while lower sedimentation rates in marine settings

181   permitted greater expression of the anaerobic reductive Acetyl-CoA pathway at depth in the

182   mat. A related possibility is that distinct microbial communities inhabited these different

183   environments. Indeed, in modern microbial mats, production of CH_4 is independent of diel

184   cycling between ambient oxic and anoxic water conditions, yet appears strongly suppressed in

185   intertidal mats and enhanced in subtidal mats as the result of differences in their anaerobic

186   community structure at depth[38]. These include differences in the activity of sulphate reducers,

187   who outcompete methanogens for organic substrates even at sulphate concentrations as low as

188   60 μM[39]. The local presence of sulphate in supratidal to braided-fluvial environments during

189   Moodies Group deposition is indicated by common pseudomorphic relics of gypsum[40] and

190   isotopic evidence for sulphate reduction in Moodies Group paleosols[14]. However, other

191   possibilities exist that may have resulted in a greater contribution of carbon from pathways

192   other than Calvin-Benson, such as the Wood-Ljungdahl pathway, in the marine realm. It has

193 been suggested that hydrogen gas was the principal electron donor for photosynthetic mat

194 growth in the 3,416 Myr Buck Reef Chert (Onverwacht Group, also in the BGB)[3,41].

195 Anoxygenic phototrophs growing on hydrogen using the reverse tricarboxylic acid or 3-

196 hydroxypropionate CO_2 fixation pathways are characterized by carbon isotope compositions

197 that tend to be heavier than -14‰ (see review in ref. 36 and references therein), for which no

198 evidence is observed in our dataset. However, if locally abundant, hydrogen might have been

199 important in stimulating anaerobic metabolism via the Wood-Ljungdahl pathway. Both

200 oxygenic and anoxygenic phototrophs may themselves produce significant quantities of

201 hydrogen gas via bi-directional hydrogenases, and under conditions of nitrogen limitation, this

202 may also occur via a nitrogenase-catalyzed side reaction[42]. In the terrestrial realm, rapid burial,

203 the increased availability of sulphate and/or fixed nitrogen, and a depressed role for hydrogen,

204 are all plausible explanations for the contrasting carbon pools preserved in the mats, however

205 it is difficult to draw further inference based on carbon isotope data alone.

206

207 **Isotopic insight into nitrogen cycling 3,220 Myr ago**

208 Bulk nitrogen isotopic compositions of mat samples also record a significant contrast between

209 the two paleoenvironments that points to differences in mat community structure and

210 respiratory processes. $\delta^{15}N$ values of marine mats range between -0.7‰ and +3.1‰, with an

211 average of +1.8‰ (n=10), in contrast to terrestrial $\delta^{15}N$ values that are generally more positive,

212 ranging between +1.9‰ and +5.6‰ with a mean of +4.3‰ (n=10, Fig. 4, Supplementary Table

213 4). The $\delta^{15}N$ values of the two sample sets are statistically different, even if the two marine data

214 points that are lowest in $\delta^{15}N$ are considered as outliers (two-tailed Welsh's t-test, p<0.002).

215 While the marine samples show near-zero values consistent with atmospheric nitrogen fixation,

216 values of up to +5‰ in the terrestrial samples are outside the range of typical fractionations

217 associated with growth on atmospheric N_2. C/N ratios range from 8 to 60 and show no

218 covariation with $\delta^{15}N$ values; similar to peak metamorphic temperatures determined by Raman

219   spectroscopy (Supplementary Table 1), C/N ratios show no significant differences between

220   terrestrial and marine mat samples (Supplementary Figure 8), suggesting that the differences

221   observed in $\delta^{15}N$ are not the expression of different diagenetic or metamorphic histories (e.g.,

222   ref. 34). Moreover, it has been shown that $\delta^{15}N$ values are resistant to modification during low

223   grade metamorphism[43], in the case of kerogen varying no more than 1‰ for sediments reaching

224   greenschist facies[44]. The lowest C/N ratios observed are probably linked to the presence of clay

225   minerals that retain nitrogen produced during diagenesis. Total nitrogen contents (12–64 ppm,

226   Supplementary Table 4) show no significant differences between marine and terrigenous

227   sediments, and show no relation to clay content (~17 to 32% illite and muscovite in samples

228   for which X-ray diffraction was performed), suggesting that variable contributions of nitrogen

229   bound to clay, including allochthonous clay, cannot explain the isotopic contrast between the

230   two datasets, which are instead most likely recording different primary compositions of mat

231   biomass.

232

233   Three different biological mechanisms are known to produce biomass with $\delta^{15}N$ compositions

234   greater than +2‰ (see ref. 45 for a detailed discussion). The first, and the only mechanism

235   possible in the absence of oxidative nitrogen cycling, is partial assimilation of NH_4^+, whereby

236   preferential uptake of $^{14}NH_4^+$ can drive the residual NH_4^+ toward isotopically heavier values

237   (e.g., ref. 46). However, only after most of the NH_4^+ pool has been assimilated would residual

238   NH_4^+ achieve values as heavy as +5‰ and we see no evidence in our dataset for light isotope

239   enrichments that would indicate this process. The two remaining hypotheses are partial

240   nitrification and/or partial denitrification, both of which require oxidative nitrogen cycling in

241   the terrestrial mats. Partial nitrification requires a local source of O_2 (with or without Mn oxide

242   intermediates) and has only been observed to generate such positive values in stratified water

243   bodies where O_2 concentrations are highly dynamic as the result of seasonal overturning[45],

244   which does not apply to the fluvial setting of the terrestrial mats. Finally, partial denitrification

245 of a stable nitrate pool is the process that is most commonly evoked for the generation of

246 isotopically heavy $\delta^{15}N$ compositions in organic matter[43,45], and would also appear to be the

247 most parsimonious explanation for the isotopically heavy $\delta^{15}N$ compositions of the terrestrial

248 mats.

249

250 The source of nitrate to the terrestrial mat ecosystem may have been atmospheric. Prebiotic

251 generation of fixed nitrogen (NO^-, NO_2^-, and NO_3^-) in the atmosphere by lightning discharge at

252 $pO_2 < 10^{-5}$ present atmospheric level (PAL) is estimated to be around 2 to 4 x 10^{11} g N per

253 year[47,48], which translates to a global surface flux of 0.1 to 0.2 μg N m^{-2} day^{-1}. While this flux

254 may have been too diffuse to be a significant source of fixed nitrogen to the marine biosphere[49],

255 fluvial mats would have had access to fixed nitrogen that is integrated over a larger area by

256 surface runoff. We calculate the drainage area required to supply an atmospheric fixed nitrogen

257 flux to mats at a rate that is comparable to that of nitrogen fixation by modern intertidal

258 microbial mats (6 to 79 mg N m^{-2} day^{-1})[50] to be only 0.02 to 0.62 km^2. In other words, rainout

259 of fixed nitrogen onto the early land surface should have had a profound influence on nitrogen

260 cycling in early terrestrial ecosystems, one that appears expressed in the contrasting nitrogen

261 isotope compositions of microbial mat biomass between terrestrial and marine settings in the

262 Moodies Group.

263

264 Our observations rejoin those from the slightly younger (~3,000 Myr) Mesoarchean fluvio-

265 lacustrine Lalla Rookh sandstone (W. Australia) where a contrast in the carbon isotope

266 composition of organic matter has also been observed[34], albeit relative to marine sediments of

267 similar age from other localities, whereas our comparison is made on approximately coeval

268 sediments from the same basin. In the Lalla Rookh sandstone, the carbon isotopic contrast

269 occurred in the reverse sense (with more important $\delta^{13}C$ depletion in lacustrine sediments) and

10

270   without any evidence for oxidative nitrogen cycling. Nonetheless, the ensemble of emerging

271   evidence indicates that microbial communities already inhabited terrestrial surface

272   environments, and fundamentally differed from their marine counterparts in their

273   biogeochemical cycling of carbon and nitrogen, at the dawn of continental emergence ca. 3,220

274   Myr ago.

References

276   1.   Nutman, A. P., Bennett, V. C., Friend, C. R. L., Van Kranendonk, M. J. & Chivas, A.
277   R. Rapid emergence of life shown by discovery of 3,700-million-year-old microbial
278   structures. *Nature* **537,** 535–538 (2016).
279   2.   Allwood, A. C., Walter, M. R., Kamber, B. S., Marshall, C. P. & Burch, I. W.
280   Stromatolite reef from the Early Archaean era of Australia. *Nature* **441,** 714–718
281   (2006).
282   3.   Tice, M. M. & Lowe, D. R. Photosynthetic microbial mats in the 3 , 416-Myr-old
283   ocean. *Nature* **431,** 549–552 (2004).
284   4.   Wacey, D., Kilburn, M. R., Saunders, M., Cliff, J. & Brasier, M. D. Microfossils of
285   sulphur-metabolizing cells in 3.4-billion-year-old rocks of Western Australia. *Nat.*
286   *Geosci.* **4,** 698–702 (2011).
287   5.   Dodd, M. S. *et al.* Evidence for early life in Earth's oldest hydrothermal vent
288   precipitates. *Nature* **543,** 60–64 (2017).
289   6.   Flament, N., Coltice, N. & Rey, P. F. The evolution of the $^{87}Sr/^{86}Sr$ of marine
290   carbonates does not constrain continental growth. *Precambrian Res.* **229,** 177–188
291   (2013).
292   7.   The term "terrestrial" has multiple definitions; here we follow convention from
293   literature on the Precambrian biosphere by considering any life on the emerged
294   continental surface, aquatic or subaerial, as terrestrial (see supplementary text).
295   8.   Beraldi-Campesi, H. Early life on land and the first terrestrial ecosystems. *Ecol.*
296   *Process.* **2,** 1 (2013).
297   9.   Wellman, C. H. & Strother, P. K. The terrestrial biota prior to the origin of land plants
298   (embryophytes): a review of the evidence. *Palaeontology* **58,** 601–627 (2015).
299   10.   Watanabe, Y., Martini, J. E. & Ohmoto, H. Geochemical evidence for terrestrial
300   ecosystems 2.6 billion years ago. *Nature* **408,** 574–578 (2000).
301   11.   Rye, R. & Holland, H. D. Life associated with a 2.76 Ga ephemeral pond?: Evidence
302   from Mount Roe #2 paleosol. *Geology* **28,** 483–486 (2000).
303   12.   Crowe, S. A. *et al.* Atmospheric oxygenation three billion years ago. *Nature* **501,** 535–
304   8 (2013).
305   13.   Mukhopadhyay, J. *et al.* Oxygenation of the Archean atmosphere: New paleosol
306   constraints from eastern India. *Geology* **42,** 923–926 (2014).
307   14.   Nabhan, S., Wiedenbeck, M., Milke, R. & Heubeck, C. Biogenic overgrowth on
308   detrital pyrite in ca. 3.2 Ga Archean paleosols. *Geology* **44,** 763–766 (2016).
309   15.   Djokic, T., Van Kranendonk, M. J., Campbell, K. A., Walter, M. R. & Ward, C. R.
310   Earliest signs of life on land preserved in ca. 3.5 Ga hot spring deposits. *Nat. Commun.*
311   **8,** 1–8 (2017).
312   16.   Javaux, E. J., Marshall, C. P. & Bekker, A. Organic-walled microfossils in 3.2-billion-
313   year-old shallow-marine siliciclastic deposits. *Nature* **463,** 934–8 (2010).
314   17.   Noffke, N., Eriksson, K. A., Hazen, R. M. & Simpson, E. L. A new window into Early
315   Archean life: Microbial mats in Earth's oldest siliciclastic tidal deposits (3.2 Ga
316   Moodies Group, South Africa). *Geology* **34,** 253 (2006).
317   18.   Heubeck, C. An early ecosystem of Archean tidal microbial mats (Moodies Group,
318   South Africa, ca. 3.2 Ga). *Geology* **37,** 931–934 (2009).
319   19.   Homann, M., Heubeck, C., Airo, A. & Tice, M. M. Morphological adaptations of 3.22
320   Ga-old tufted microbial mats to Archean coastal habitats (Moodies Group, Barberton
321   Greenstone Belt, South Africa). *Precambrian Res.* **266,** 47–64 (2015).
322   20.   Homann, M. *et al.* Evidence for cavity-dwelling microbial life in 3.22 Ga tidal
323   deposits. *Geology* **44,** 51–54 (2016).
324   21.   Eriksson, K. A., Simpson, E. L. & Mueller, W. U. An unusual fluvial to tidal transition

325		in the mesoarchean Moodies Group, South Africa: A response to high tidal range and
326		active tectonics. *Sediment. Geol.* **190,** 13–24 (2006).
327	22.	Heubeck, C. *et al.* Geological constraints on Archean (3.22 Ga) coastal-zone processes
328		from the Dycedale Syncline, Barberton Greenstone Belt. *South African J. Geol.* **119,**
329		495–518 (2016).
330	23.	De Ronde, C. E. J. & Kamo, S. L. An Archaean arc-arc collisional event: A short-lived
331		(ca 3 Myr) episode, Weltevreden area, Barberton greenstone belt, South Africa. *J.*
332		*African Earth Sci.* **30,** 219–248 (2000).
333	24.	Heubeck, C. *et al.* Timing of deposition and deformation of the Moodies Group
334		(Barberton Greenstone Belt, South Africa): Very-high-resolution of Archaean surface
335		processes. *Precambrian Res.* **231,** 236–262 (2013).
336	25.	Farber, K., Dziggel, A., Trumbull, R. B., Meyer, F. M. & Wiedenbeck, M. Tourmaline
337		B-isotopes as tracers of fluid sources in silicified Palaeoarchaean oceanic crust of the
338		Mendon Formation, Barberton greenstone belt, South Africa. *Chem. Geol.* **417,** 134–
339		147 (2015).
340	26.	Xie, X., Byerly, G. R. & Ferrell Jr., R. E. IIb trioctahedral chlorite from the Barberton
341		greenstone belt: crystal structure and rock composition constraints with implications to
342		geothermometry. *Contrib. to Mineral. Petrol.* **126,** 275–291 (1997).
343	27.	Tice, M. M., Bostick, B. C. & Lowe, D. R. Thermal history of the 3.5–3.2 Ga
344		Onverwacht and Fig Tree Groups, Barberton greenstone belt, South Africa, inferred by
345		Raman microspectroscopy of carbonaceous material. *Geology* **32,** 37 (2004).
346	28.	Popp, B. N. *et al.* Effect of Phytoplankton Cell Geometry on Carbon Isotopic
347		Fractionation. *Geochim. Cosmochim. Acta* **62,** 69–77 (1998).
348	29.	Hayes, J. M., Strauss, H. & Kaufman, A. J. The abundance of in marine organic matter
349		and isotopic fractionation in the global biogeochemical cycle of carbon during the past
350		800 Ma. *Chem. Geol.* **161,** 103–125 (1999).
351	30.	Driese, S. G. *et al.* Neoarchean paleoweathering of tonalite and metabasalt:
352		Implications for reconstructions of 2.69Ga early terrestrial ecosystems and
353		paleoatmospheric chemistry. *Precambrian Res.* **189,** 1–17 (2011).
354	31.	Laws, E. A., Popp, B. N., Cassas, N. & Tanimoto, J. ^{13}C discrimination patterns in
355		oceanic phytoplankton: likely influence of CO_2 concentrating mechanisms, and
356		implications for palaeoreconstructions. *Funct. plant Biol.* **29,** 323–333 (2002).
357	32.	Schidlowski, M. A 3,800-million-year isotopic record of life from carbon in
358		sedimentary rocks. *Nature* **333,** 313–318 (1988).
359	33.	Eigenbrode, J. L. & Freeman, K. H. Late Archean rise of aerobic microbial ecosystems.
360		*Proc. Natl. Acad. Sci.* **103,** 15759–15764 (2006).
361	34.	Stüeken, E. E. & Buick, R. Environmental control on microbial diversification and
362		methane production in the Mesoarchean. *Precambrian Res.* **304,** 64–72 (2018).
363	35.	Slotznick, S. P. & Fischer, W. W. Examining Archean methanotrophy. *Earth Planet.*
364		*Sci. Lett.* **441,** 52–59 (2016).
365	36.	Havig, J. R., Hamilton, T. L., Bachan, A. & Kump, L. R. Sulfur and carbon isotopic
366		evidence for metabolic pathway evolution and a four-stepped Earth system progression
367		across the Archean and Paleoproterozoic. *Earth-Science Rev.* **174,** 1–21 (2017).
368	37.	Baumgartner, L. K. *et al.* Sulfate reducing bacteria in microbial mats: Changing
369		paradigms, new discoveries. *Sediment. Geol.* **185,** 131–145 (2006).
370	38.	Hoehler, T. M., Bebout, B. M. & Des Marais, D. J. The role of microbial mats in the
371		production of reduced gases on the early Earth. *Nature* **412,** 324–327 (2001).
372	39.	Lovley, D. R. & Klug, M. J. Sulfate reducers can outcompete methanogens at
373		freshwater sulfate concentrations. *Appl. Environ. Microbiol.* **45,** 187–92 (1983).
374	40.	Nabhan, S., Luber, T., Scheffler, F. & Heubeck, C. Climatic and geochemical
375		implications of Archean pedogenic gypsum in the Moodies Group (~3.2Ga), Barberton

376   Greenstone Belt, South Africa. *Precambrian Res.* **275,** 119–134 (2016).

377   41.   Tice, M. M. & Lowe, D. R. Hydrogen-based carbon fixation in the earliest known

378   photosynthetic organisms. *Geology* **34,** 37 (2006).

379   42.   Bandyopadhyay, A., Stöckel, J., Min, H., Sherman, L. A. & Pakrasi, H. B. High rates

380   of photobiological H2 production by a cyanobacterium under aerobic conditions. *Nat.*

381   *Commun.* **1,** 139 (2010).

382   43.   Ader, M. *et al.* Interpretation of the nitrogen isotopic composition of Precambrian

383   sedimentary rocks: Assumptions and perspectives. *Chem. Geol.* **429,** 93–110 (2016).

384   44.   Ader, M. *et al.* Nitrogen isotopic evolution of carbonaceous matter during

385   metamorphism: Methodology and preliminary results. *Chem. Geol.* **232,** 152–169

386   (2006).

387   45.   Stüeken, E. E. A test of the nitrogen-limitation hypothesis for retarded eukaryote

388   radiation: Nitrogen isotopes across a Mesoproterozoic basinal profile. *Geochim.*

389   *Cosmochim. Acta* **120,** 121–139 (2013).

390   46.   Papineau, D. *et al.* High primary productivity and nitrogen cycling after the

391   Paleoproterozoic phosphogenic event in the Aravalli Supergroup, India. *Precambrian*

392   *Res.* **171,** 37–56 (2009).

393   47.   Kasting, J. F. & Walker, J. C. G. Limits on oxygen concentration in the prebiological

394   atmosphere and the rate of abiotic fixation of nitrogen. *J. Geophys. Res.* **86,** 1147

395   (1981).

396   48.   Navarro-gonz, R., Molina, M. J. & Molina, L. T. Nitrogen fixation by volcanic

397   lightning in the early Earth. *Geophys. Res. Lett.* **25,** 3123–3126 (1998).

398   49.   Stüeken, E. E., Kipp, M. A., Koehler, M. C. & Buick, R. The evolution of Earth's

399   biogeochemical nitrogen cycle. *Earth-Science Rev.* **160,** 220–239 (2016).

400   50.   Joye, S. B. & Paerl, H. W. Nitrogen Cycling In Microbial Mats - Rates And Patterns Of

401   Denitrification And Nitrogen-Fixation. *Mar. Biol.* **119,** 285–295 (1994).

402

403

404   **Corresponding author**

405   Correspondence and request for materials should be addressed to M.H.

406   (martin.homann@univ-brest.fr)

407

Author contributions

M.H. and C.H. carried out field work and collected samples in South Africa. P.S., M.A., and

S.V.L. helped with the acquisition and interpretation of elemental and isotopic data. M.V.Z.

and J.G. performed Raman analysis. B.K., I.S.F., A.A. and M.J.V.K. contributed to the

discussion of the data. M.H. wrote the manuscript with significant contributions from all co-

authors.
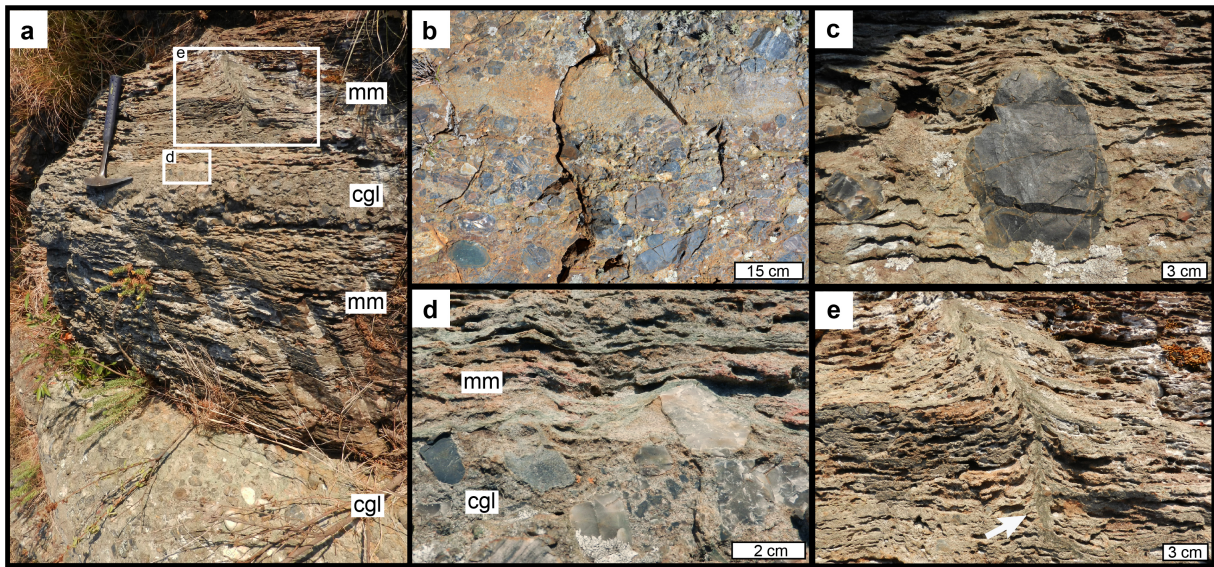
Figures

Figure 1. Field photographs of fluvial sandstones and conglomerates hosting fossil terrestrial mats from the 3,220 Myr old Moodies Group. a, Overview photograph showing interbedded fossil microbial mats (mm) and conglomerates (cgl). **b**, Mat-associated fluvial conglomerate, composed of subrounded pebbles and cobbles. **c, d**, Microbial mats draping and onlapping interbedded clasts within the sandstones and on top of conglomerate beds (close-up view of the framed area in (a). **e**, Fluid-escape structure with well-defined central channel (arrow) that vertically disrupts the densely mat-laminated sandstone (close-up view of the framed area in (a).
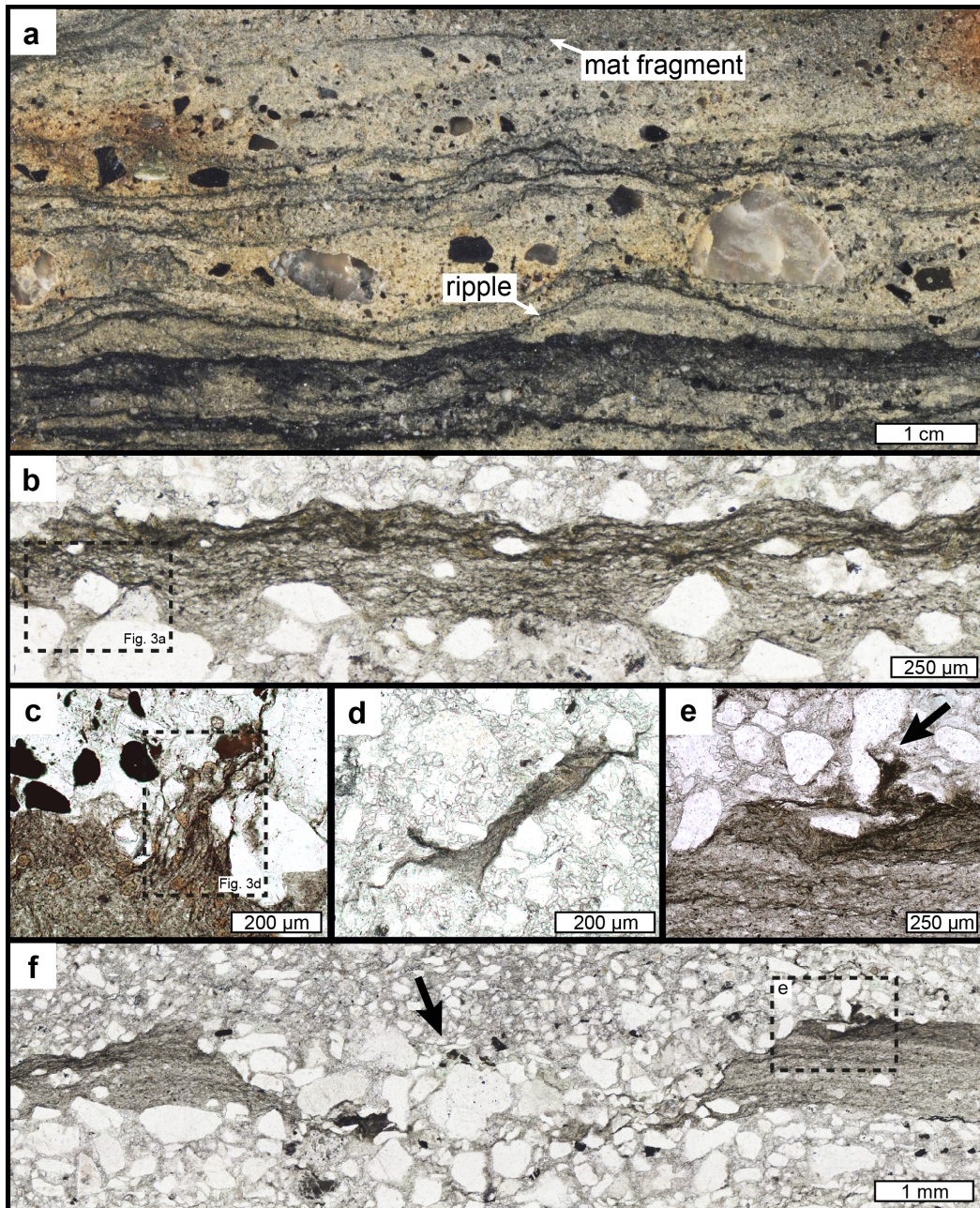
Figure 2. Reflected and transmitted light photomicrographs of the terrestrial microbial mats of the Moodies Group. a, Dark carbonaceous laminae of the fossil mats draping horizontally laminated and rippled sand and onlapping pebbles. Chips of eroded mat fragments are preserved in cross-laminated, granular sandstone. **b,** Dense meshwork of interwoven filamentous microstructures with trapped detrital grains. **c**, Bundled filamentous structures in upper part of the mat. **d**, Close-up view of eroded mat fragment. **e,** Partially eroded microbial mat laminae due to abrasion by impacting sand grains (arrow) and **f,** Erosional truncation of the mat by small channel (arrow).
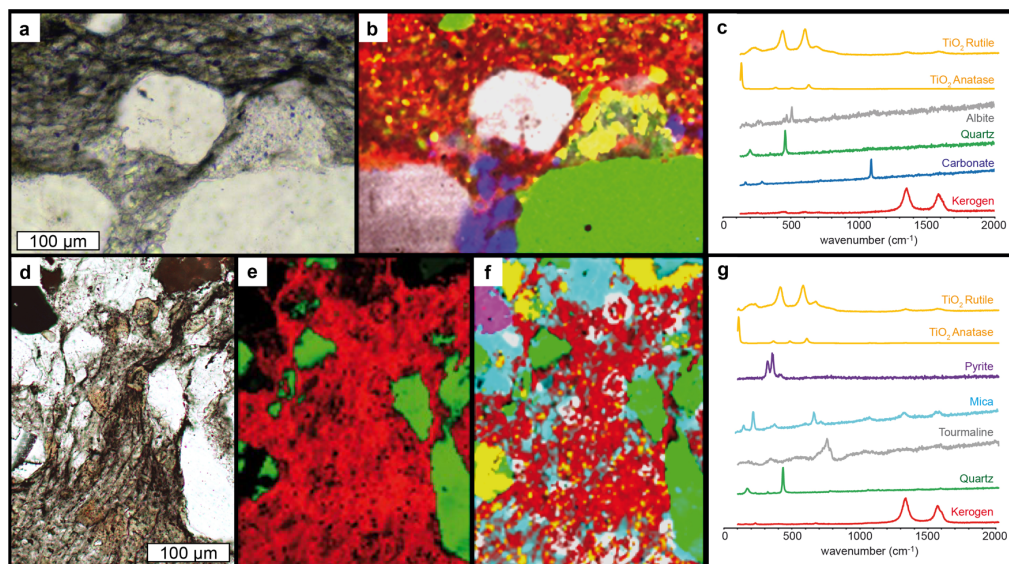
Figure 3. Transmitted light photomicrographs of preserved kerogenous laminae (a) and filamentous microstructures (d) of the terrestrial mats, with corresponding Raman component maps for mineral phases and G-peak intensity for kerogenous phases (**b, e, f**), and representative Raman component spectra (**c, g**). Note that the analyzed areas are close-up views of the samples shown in Figure 2B and 2C, respectively.
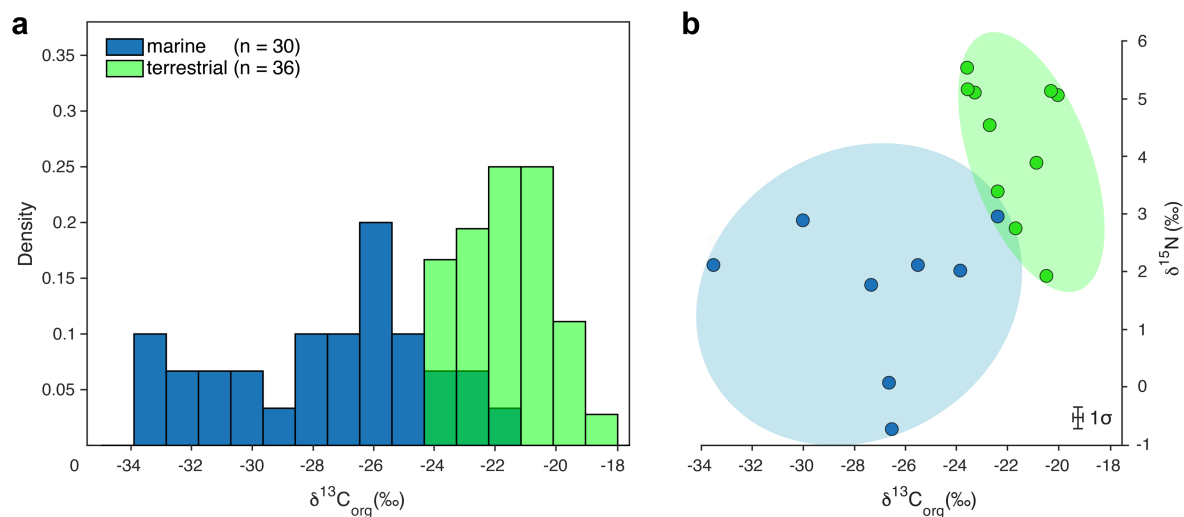
Figure 4. Carbon isotope composition of organic matter and bulk nitrogen isotope composition from terrestrial (green) and marine (blue) microbial mats of the Paleoarchean Moodies Group. a, Histogram of organic carbon $\delta^{13}C_{org}$ and **b,** $\delta^{13}C_{org}$ versus $\delta^{15}N$ values for both environments.

17

Methods

Optical microscopy. Standard 30-μm-thick, polished thin sections, oriented perpendicular to bedding, were analyzed using an Olympus BX60 petrographic microscope and a Zeiss Axio Scope.A1 equipped with a 63x oil objective lens. High resolution scans of entire thin sections were performed with a Zeiss Axio Zoom v16 motorized stereo microscope at the IPGP, Paris.

Raman spectroscopy. Raman analyses were performed using a Renishaw InVia Raman microscope coupled to an Olympus BX61 Confocal microscope, within the PARI analytical platform at the IPGP in Paris. Measurements were made with a 514 nm-excitation (Ar-ion laser) and adjusted to an on-sample intensity of 0.2 mW with a spot size of < 2 μm (50x objective). Beam centering and Raman spectral calibration were performed on a pure silicon chip with a specific Raman band at 520.4 cm^{-1}. All spectra were detected using 1800 l/mm grating, and a detector configuration in streamspot mode, providing a spectral range of 2000 cm^{-1} in static mode. Individual spot analyses were obtained in both static mode (2 x 20 s exposure, centered at 1150 cm^{-1} with a spectral range of 100-2000 cm^{-1}) and extended mode (1 x 20 s exposure, spectral range 100-4000 cm^{-1}). In order to determine Raman spectral indicators of the carbonaceous fractions, the individual spectra were truncated to 900-1900 cm^{-1}, and a linear background subtraction was performed, using the program Wire 2.0. Peak-decomposition was performed using two generally reported methods: a) a 2-peak fit, assigning a D-peak at ca. 1350 cm^{-1} and a G-peak at ca. 1600 cm^{-1} (following the procedure outlined in Sforna et al.[51]), b) a 4-peak fit, assigning a D1-, D2-, D3-, and G-peak at ca. 1350 cm^{-1}, 1620 cm^{-1}, 1500 cm^{-1}, and 1600 cm^{-1}, respectively (following the procedure outlined in Sforna et al.[51], Supplementary Fig. 6). In all obtained spectra a D4-peak at ca. 1200 cm^{-1} was absent and was therefore not assigned during the peak decomposition procedure. Spectral data of the decomposed peaks (position, width, height, area) were recorded and used for calculating the Raman indicators D-FWHM (D-peak full width at half maximum) and ID/IG (height-based D/G) using the 2-peak fit, and D1-

18

481 FWHM, R1 (height-based D1/G) and R2 (area-based D1/D1+D2+G) using the 4-peak fit. Two

482 geothermometers could then be calculated, that of Beyssac et al.[52] using T= -445xR2 + 641,

483 and that of Kouketsu et al.[53] using T= (-2.15 x D1-FWHM) + 478 (see Supplementary Table

484 1). Raman hyperspectral maps were obtained for selected areas within the thin sections 14-452-

485 1B2 and 14-452-1B9, in streamspot mode (point-by-point scanning) using 1 x 6 s or 1 x 10 s

486 exposures per point. Raman maps were generated using the software Wire 2.0 by selecting

487 representative spectra for each component (minerals and kerogen) within the hyperspectral

488 dataset (Fig. 3) and subsequent component analysis for each spectral point was determined

489 using a background subtraction with a 2nd order polynomial fit. Maps of individual components

490 were subsequently merged using the imaging program ImageJ.

491

492 **Carbon isotope analysis.** For isotope analysis of organic carbon, large rock samples (up to

493 50x20 centimeters) were collected in the field from the freshest and least weathered outcrops

494 available. In the lab all outer surfaces of the rocks where removed with a rock saw and were

495 cut into smaller blocks, devoid of any cracks or fractures. Afterwards, mat horizons, 2 – 10 mm

496 thick, were cut out individually with a thin rock saw and broken into smaller pieces, cleaned in

497 an ultrasonic bath and dried. The resultant material was then crushed into a fine powder using

498 an automated agate mill grinder, which was cleaned with pure quartz sand, distilled water, and

499 ethanol between each run. The powders were decarbonated with 6N HCl for 12 hours then

500 warmed at 80°C for 2h in a fume hood. Residues were rinsed with Milli-Q water, then

501 centrifuged three to four times until they approached a neutral pH. 10 to 50 mg of decarbonated

502 samples were loaded into tin capsule and analyzed for their carbon isotopic composition at the

503 Pôle Spectométrie Océan (PSO, Brest, France) using a Thermo Scientific Delta V plus mass

504 spectrometer coupled to a Flash 2000 elemental analyzer. Isotopic results are reported in delta

505 notation against the V-PDB standard (Vienna Pee Dee Belemnite) with an average analytical

506 error of 0.12‰ (2σ, Supplementary Table 3). For C and O isotope composition of the mat-

507   associated carbonates, CO_2 was released from powdered samples by reaction with 100% H_3PO_4

508   at 72ºC in a Kiel IV automated carbonate preparation device. The CO_2 was analyzed using for

509   isotope compositions using a Finnigan MAT 253 mass spectrometer. $^{18}O/^{16}O$ and $^{13}C/^{12}C$ ratios

510   were also expressed in delta notation relative to the V-PDB standard (Supplementary Table 2).

511   Precision for $\delta^{18}O$ and $\delta^{13}C_{carb}$ was 0.2‰ (2σ) and 0.1‰ (2σ), respectively.

512

513   **Nitrogen isotope analysis.** Individual carbonaceous mat laminae were manually separated

514   from fresh and unweathered sandstone samples (as described above), ground in an automated

515   agate mill grinder, and sieved to ensure a grain size smaller than 140 μm. Bulk rock $\delta^{15}N$

516   measurements were performed as they have been suggested to be more likely to record the

517   primary isotopic composition of the original biomass in kerogen-poor greenschist-facies

518   metasediments as compared to measurements of kerogen isolates[54]. To concentrate nitrogen in

519   the insoluble residue, the samples were first decarbonated in HCl 6N for 12h overnight at room

520   temperature, followed by 2h at 80°C in a fume hood. Residual material was rinsed three times

521   with Milli-Q water, then centrifuged and dried at 50°C overnight. Approximately 500-1400 mg

522   of powdered samples were analyzed following the method detailed in Ader et al.[55].

523   Conventional sealed tube combustion with CuO_2 and Cu rods (but in this study without CaO

524   grains) was used to convert total nitrogen to N_2 (Dumas combustion), which was then purified

525   using a secondary vacuum extraction line as shown in Figure 1 of Li et al.[56] N_2 nitrogen isotope

526   ratio measurements were performed using a dual inlet Thermo-Fisher Delta V+ mass

527   spectrometer at the IPGP in Paris (Supplementary Table 4). Each purified nitrogen gas sample

528   was analyzed twice. Nitrogen blanks were lower than 0.1 micromoles, thus representing less

529   than 10% of the measured nitrogen. External reproducibility of the $\delta^{15}N_{sed}$ measurements was

530   ± 0.4 ‰ (1σ).

531

532   **Data availability.** The authors declare that all data supporting the study are available within

533   the article and its Supplementary Information file.

534

535   **References**

536   51.   Sforna, M. C., van Zuilen, M. A. & Philippot, P. Structural characterization by Raman
537   hyperspectral mapping of organic carbon in the 3.46 billion-year-old Apex chert,
538   Western Australia. *Geochim. Cosmochim. Acta* **124,** 18–33 (2014).
539   52.   Beyssac, O., Goffé, B., Chopin, C. & Rouzaud, J. N. Raman spectra of carbonaceous
540   material in metasediments: a new geothermometer. *J. Metamorph. Geol.* **20,** 859–871
541   (2002).
542   53.   Kouketsu, Y. *et al.* A new approach to develop the Raman carbonaceous material
543   geothermometer for low-grade metamorphism using peak width. *Isl. Arc* **23,** 33–50
544   (2014).
545   54.   Stüeken, E. E., Zaloumis, J., Meixnerová, J. & Buick, R. Differential metamorphic
546   effects on nitrogen isotopes in kerogen extracts and bulk rocks. *Geochim. Cosmochim.
547   Acta* **217,** 80–94 (2017).
548   55.   Ader, M., Boudou, J.-P., Javoy, M., Goffe, B. & Daniels, E. Isotope study on organic
549   nitrogen of Westphalian anthracites from the Western Middle field of Pennsylvania
550   (U.S.A.) and from the Bramsche Massif (Germany). *Org. Geochem.* **29,** 315–323
551   (1998).
552   56.   Li, L., Cartigny, P. & Ader, M. Kinetic nitrogen isotope fractionation associated with
553   thermal decomposition of NH3: Experimental results and potential applications to trace
554   the origin of N2 in natural gas and hydrothermal systems. *Geochim. Cosmochim. Acta*
555   **73,** 6282–6297 (2009).
556

557

558